Development of organic/inorganic PANI/ZnO 1D nanostructured hybrid thin film solar cell by soft chemical route

Published: 06 August 2019

Volume 30, pages 16056–16064, (2019) Cite this article

Journal of Materials Science: Materials in Electronics

Aims and scope

Submit manuscript

Dipak A. Tonpe, Ketan P. Gattu, Vishnu V. Kutwade, Makrand E. Sonawane, Avinash S. Dive & Ramphal Sharma

Abstract

Polyaniline (PANI)/zinc oxide (ZnO) nanorods hybrid solar cell device was fabricated via a two-step process. The first step involved soft chemical synthesis of ZnO nanorods thin film on the indium-doped tin oxide (ITO) substrate and subsequent annealing in air at 300 °C. The second step of involved chemisorption of PANI on the surface of the ZnO nanorods by Doctor Blade Method. The fabricated heterojunction films were characterized

by X-ray diffraction (XRD), field emission scanning electron microscope (FE-SEM), fourier transform infrared (FT-IR), and Raman spectra. The results confirmed chemical interactions between PANI and ZnO and thus the formation of the heterojunction. Both the PANI coated pristine and annealed ZnO nanorods thin films were studied for their solar cell characteristics. The results of solar cell measurements showed that the overall light-conversion efficiency of PANI coated pristine ZnO thin film to be ~ 80% higher than for PANI coated annealed ZnO thin film. This is attributed to more effective charge separation and faster interfacial charge transferring occurred in the pristine ZnO thin films.

1 Introduction

One of the most promising ways to tackle today's energy issues is harnessing solar energy. The photovoltaic (PV) technology based on inorganic materials has limited acceptance in the market due to its high material and manufacturing costs [1]. Organic photovoltaic (OPV) devices are one of the low-cost alternative PV technologies; these devices are based on organic semiconductors [2]. But these narrow bandgap semiconductor nanostructures provide low photocurrent as fast charge recombination limits the photocurrent generation [3]. The recent development in metal-polymer or

metal oxide-polymer hybrid nanomaterials in organic/inorganic hybrid solar cells has reported ultra-fast photoinduced charge transfer between a conjugated polymer and a metal oxide semiconductors [4], among these ZnO is considered to be a very promising material due to its large exciton binding energy (60 MeV), direct wide bandgap in the near-UV spectral region along with the ability to form diverse morphologies such as nanorods, thin films, nanoflakes, nanowires, nanoplates, etc. Various techniques have been established to deposit the ZnO thin films such as molecular beam epitaxy (MBE), R. F sputtering, PLD sol–gel, chemical vapor deposition (CVD), and metal–organic chemical vapor deposition (MOCVD), SILAR, Soft Chemical Route etc. [5]. Among all of these soft chemical technique is considered to be one of the most economic techniques to grow the thin film because of the excellent stoichiometric transfer of the material from the solution to the substrate [6].

Furthermore, the One-dimensional nanostructures (e.g. nanorods, nanowires, and nanotubes) have been found to be excellent in solar cells device applications as they provide a direct conduction pathway for the rapid collection of photo-generated electrons, however most of this 1D-nanostructured ZnO-based in solar cells have a low current density due to low surface interaction with the dye thus exhibiting low light harvesting [7]. In order to increase the surface interaction and surface area of 1D-nanostructured ZnO the thin films have been annealed by many authors which resulted in increased nanorods length and thus higher surface interaction [8, 9].

On the other hand Polymers such as polythiophene, polyaniline and polypyrrole have been investigated for their applications in energy storage and conversion devices. Among these, polyaniline (PANI) as an organic polymer have many advantages such as easy preparation, environmental stability, and high conductivity [10]. Polyaniline is reported as a hole injecting layer and as a planarizing layer to inhibit electrical shorts in organic light emitting diodes (LEDs) wherein it acts as a barrier to oxygen and improves device lifetime, resulting in an increase in the efficiency of the organic LEDs [11].

Thus with an aim to utilize the ultrafast photo induced charge carrier transfer by 1D nanorods morphology of ZnO along with maintaining the solution processability and thus high throughput, low cost device production. Herein, we report the PANI/ZnO hybrid solar cell with 1D ZnO nanorods thin film synthesized using soft chemical route and the PANI synthesized by the chemical polymerization method. Furthermore, the effect of

annealing the ZnO thin film on the performance of PANI/ZnO hybrid solar cell is discussed in detail.

2 Experimental procedure

2.1 Materials

The chemicals like Ammonium Peroxydisulphate (APS), HCl, Aniline, were purchased from Merck. The chemicals were of analytical grades and used without further purification. Zinc acetate dehydrate ($ZnC_4H_6O_4{\cdot}2H_2O$), Ammonia (NH_3), Thiourea (CH_4N_2S) and TEA (tri-ethanolamine- $C_6H_{15}NO_3$) of AR grade were purchased from Merck. ITO slides were thoroughly washed using soap solution, ultrasonicated for 15 min in isopropanol, then for 15 min in soap solution. Finally, the slides were cleaned with soap solution till a uniform water film is seen on the ITO surface indicating the ITO surface to be well cleaned.

2.2 Synthesis of ZnO nanorods thin film

ZnO nanorods thin film was prepared by dissolving 1.31 g Zinc Acetate in 30 ml of DI water, 4 drops of tri-ethanolamine- $C_6H_{15}NO_3$ (TEA) were added to the Zinc Acetate solution which turns the solution milky white, Ammonia was then added dropwise with continuous stirring to make the solution transparent. 0.91 g of Thiourea (CH_4N_2S) was dissolved in 30 ml deionized water in a separate beaker. When both solutions were completely transparent, they were mixed together in a beaker and two pre-cleaned ITO substrates were placed into the solution. The bath temperature was maintained at 85 °C for 45 min.

After 45 min. ZnO nanorod thin film deposited ITO substrates were removed and washed with DI water. ZnO deposited thin film was air dried. One of the two thin films was annealed at 300 °C for 2 h. The annealing temperature was selected as 300 °C as above this temperature the ITO substrate may undergo degradation [12,13,14,15].

2.3 Synthesis of PANI

Polyaniline was synthesized by dissolving 1 M of aniline in 50 mL DI water then 4 ml of 1 M HCl was added to it at room temperature and stirred for 15 min. 0.5 M Ammonium Peroxydisulphate (APS) was dissolved in 50 ml DI water in a separate beaker and stirred for 15 min. Both these solutions were then cooled to ~ 4 °C for 45 min. Thereafter both the solutions were mixed together and stirred for 2 h. The oxidative polymerization of aniline

with APS in the presence of HCl shows an exothermic nature of the reaction which can be observed by monitoring the reaction temperature. The initial temperature of the reaction was ~ 4 °C and the final temperature became ~ 34 °C. Increase in the temperature confirms the exothermic nature of the reaction. The pH of the reaction bath decreases continuously this may be attributed to the increase in H^+ ion concentration in the reaction bath. Upon protonation, the imine group of quinoid ring gets transformed into semiquinone radical cation. This leads to the addition of H^+ ion into the reaction. Initial pH of the reaction bath was ~ 1.06 and at the completion of the reaction, it became ~ 0.6. The stepwise decrease in pH indicates an increase in doping level. The obtained powder was then washed with DI water and air dried.

2.4 Devices fabrication

Solar cell device was fabricated by coating the PANI powder over the ZnO deposited ITO substrate. For this, the filtered PANI powder was washed with DI water multiple times to reduce the pH of the PANI powder; this was then ground to form a uniform paste. This paste was then uniformly coated over ZnO thin films using the doctor-blade method. The PANI coated ZnO thin film samples were then air dried at room temperature for 12 h. The ITO substrate acted as a back contact and silver contacts were made onto coated PANI films using silver paste.

2.5 Characterizations

The synthesized nanocrystalline ZnO nanorods thin films were investigated using X-ray diffraction (XRD). The XRD spectra of ZnO thin film were recorded using Bruker D8 Advance X-ray diffractometer. The X-rays were produced using a sealed tube and the wavelength of X-ray was 0.154 nm (Cu $K_{\alpha 1}$ radiation) for 20 °C to 80 °C. The X-rays were detected using a fast counting detector based on Silicon strip technology (Bruker Lynx Eye detector). The morphology of Pristine and annealed ZnO films were investigated using Field Emission Scanning Electron Microscopy (FE-SEM, JEOL JSM 5600). The samples were sputter coated with Au to avoid charging effect. Atomic force microscopic (AFM) images of the films were probed by an atomic force microscope (Park Systems, Model: NX20) in the tapping mode. The Raman spectra of the samples were recorded using Micro Raman system from Jobin–Yvon Horibra LABRAM-HR. Raman spectra was recorded from 200 cm^{-1} to 1800 cm^{-1} of Raman shift; Argon 488 nm excitation wavelength was used. The characteristics functional groups of the samples were investigated using FTIR spectra recorded using FTIR (CARRY 600Z series, Japan). The

Perkin Elmer Lambda 25 UV–Vis Spectrophotometer was used to obtain UV–Vis absorption spectra. The current–voltage (I–V) measurements were performed using a computer interfaced Keithley 2400 source meter.

3 Results and discussions

3.1 Structural analysis

3.1.1 XRD analysis

Figure 1 shows the XRD patterns for the ZnO NRs (a) Pristine and (b) annealed at 300 °C synthesized by soft chemical route. The prepared samples revealed pronounced diffraction peaks consistent with the wurtzite structure of ZnO (JCPDS No. 01-080-0074). The diffraction peaks were observed for (100), (002), (101), (102), (110), (103), and (112) with a dominant sharp peak at $2\theta = 34.43°$ corresponding to (002) plane confirming the c-axis-oriented growth in [0001] direction [16]. This resulted in vertical growth of ZnO nanorods on the substrate surface. On comparison of peak intensities for indexed planes viz. (100), (002) and (101) we observe that the peak intensity for (100) plane remained constant, while that for (002) and (101) got decreased after annealing. These changes in the peak intensity suggest the decrease in nanorods length as well as transformation of nanorods tip to planar surface [16, 17]. The average Crystallite size (D) for the ZnO-NRs thin films was calculated using the Debye–Scherrer's formula $D = 0.9\lambda/\beta\cos\theta$, where λ is the wavelength of X-rays (1.506 Å) and β is the full width at half maxima (FWHM).

Fig. 1

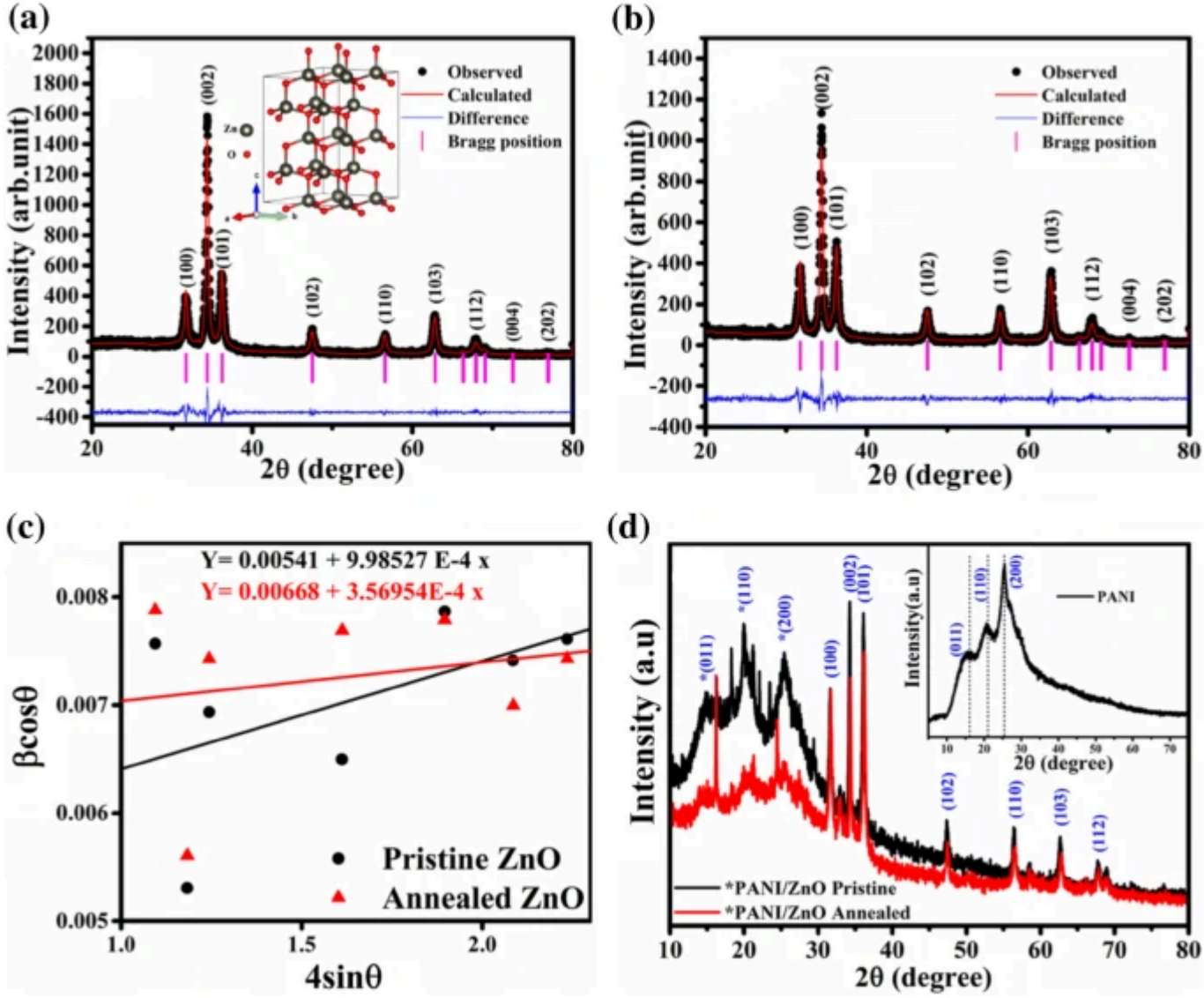

Rietveld refinement of **a** Pristine ZnO, **b** 300 °C annealed ZnO thin film **c** WH-analysis of pristine and annealed ZnO thin films and **d** XRD patterns of PANI/pristine ZnO and PANI/annealed ZnO thin film

The calculated average crystallite size value for the as-grown and annealed ZnO-NRs was found to be 20 nm and 19 nm respectively. Also to determine the effect of strain on the crystallite size, the strain and crystallite size were calculated using W–H analysis method [18]. The obvious significant decrease in strain was observed along with a decrease in crystallite size after annealing. The calculated value of strain was found to be 0.001 and 0.00035 for pristine and annealed ZnO thin film respectively, also the crystallite size from W–H analysis was found to be 25.63 nm and 20.76 nm for pristine and annealed ZnO thin films respectively. The decrease in crystallite size along with the decrease in length of nanorods can be attributed to the removal of water molecules i.e. conversion of $Zn(OH)_2$ to

ZnO. All the crystallographic parameters calculated from the XRD patterns are tabulated in Table 1.

Table 1 Crystallographic parameters calculated from the XRD patterns

Figure 1d (inset) shows three characteristic peaks of pure PANI thin film. The peaks centered at $2\theta = 15.6°$, 20.3° and 25.7° ascribe to the (011), (110) and (200) planes of the orthorhombic unit cell of PANI [19]. The diffraction peak centered at $2\theta = 25.7°$, is assigned to the scattering from PANI chains at interplanar spacing [19]. These peaks can be clearly seen in the PANI coated ZnO samples confirming the formation of PANI/ZnO bilayer.

3.2 Morphological analysis

3.2.1 Field emission scanning electron microscopy (FE-SEM)

The surface morphology of the pristine ZnO and annealed ZnO thin films were examined by FE-SEM. The FE-SEM images of the both pristine and annealed ZnO thin films deposited onto the ITO substrates by soft chemical route along with the corresponding high-resolution view (inset) is shown in Fig. 2a and b respectively.

Fig. 2

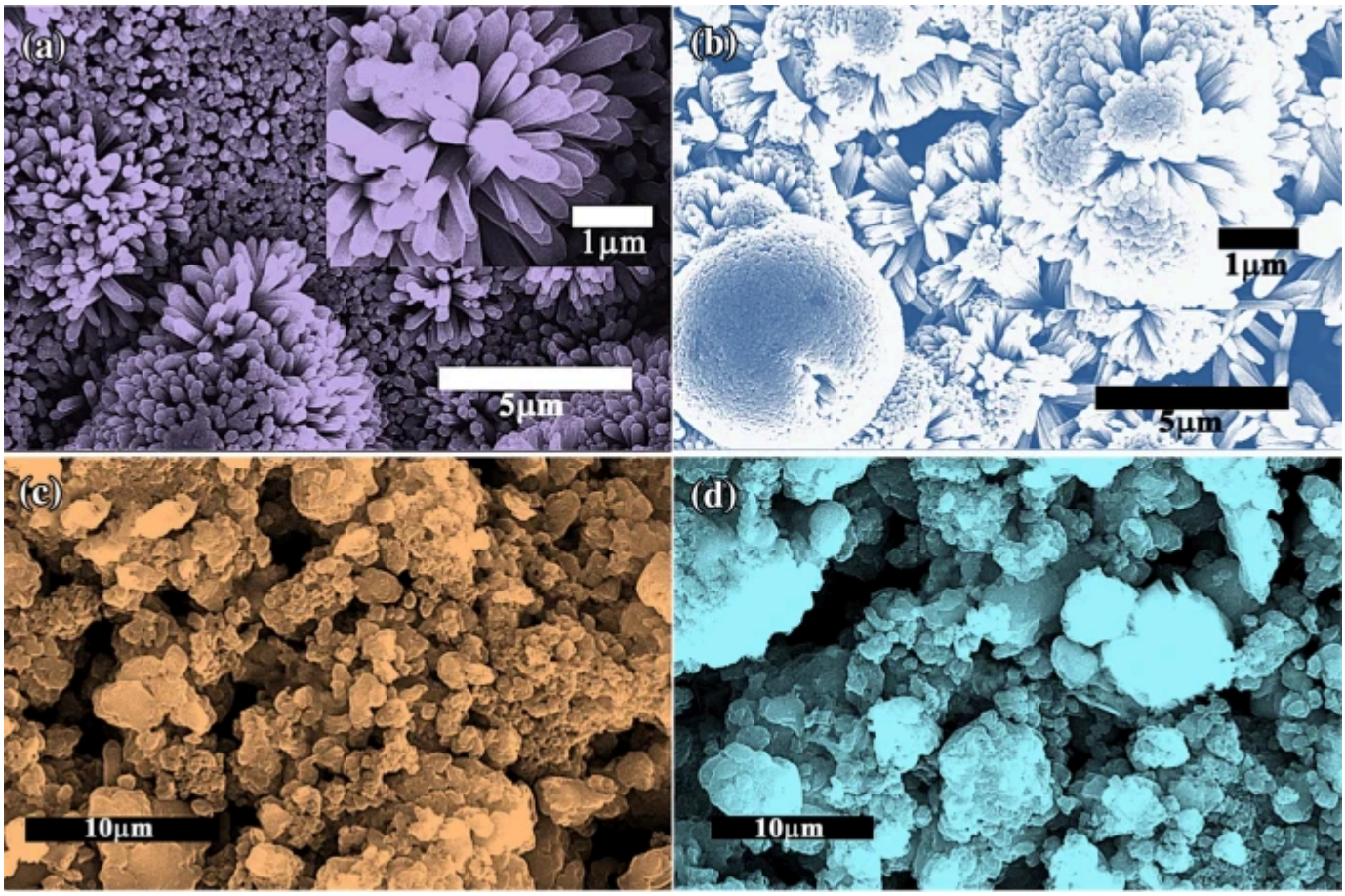

FE-SEM images of ZnO thin film **a** Pristine ZnO, **b** annealed ZnO, **c** PANI coated pristine ZnO and **d** PANI coated annealed ZnO thin film

From the Fig. 2a we observe well-defined ZnO nanorods grown over the substrate surface with needle like tip, these nanorods get very close horizontally with decrease in nanorod length and the needle like tip transformed to blunt planar surface when annealed at 300 °C Fig. 2b. This change in morphology of the nanorods resulted in the decrease in peak intensity along (002) and (101) planes in XRD pattern. Figure 2c and d shows the PANI coated pristine and ZnO thin films. The uniform coating of PANI over ZnO thin film covered the ZnO nanorods.

3.2.2 Atomic force microscopy (AFM)

Figure 3 shows the AFM images of pristine, annealed ZnO thin films and PANI coated pristine and annealed ZnO thin films. From Fig. 3a we can clearly see nanorods like morphology of the pristine ZnO thin film, the nanorods length got reduced with annealing at 300 °C as can be seen from Fig. 3b, also confirmed from the XRD and FE-SEM results. From the Fig. 3c and d we can see the change in morphology depicting the ZnO nanorods covered with PANI.

Fig. 3

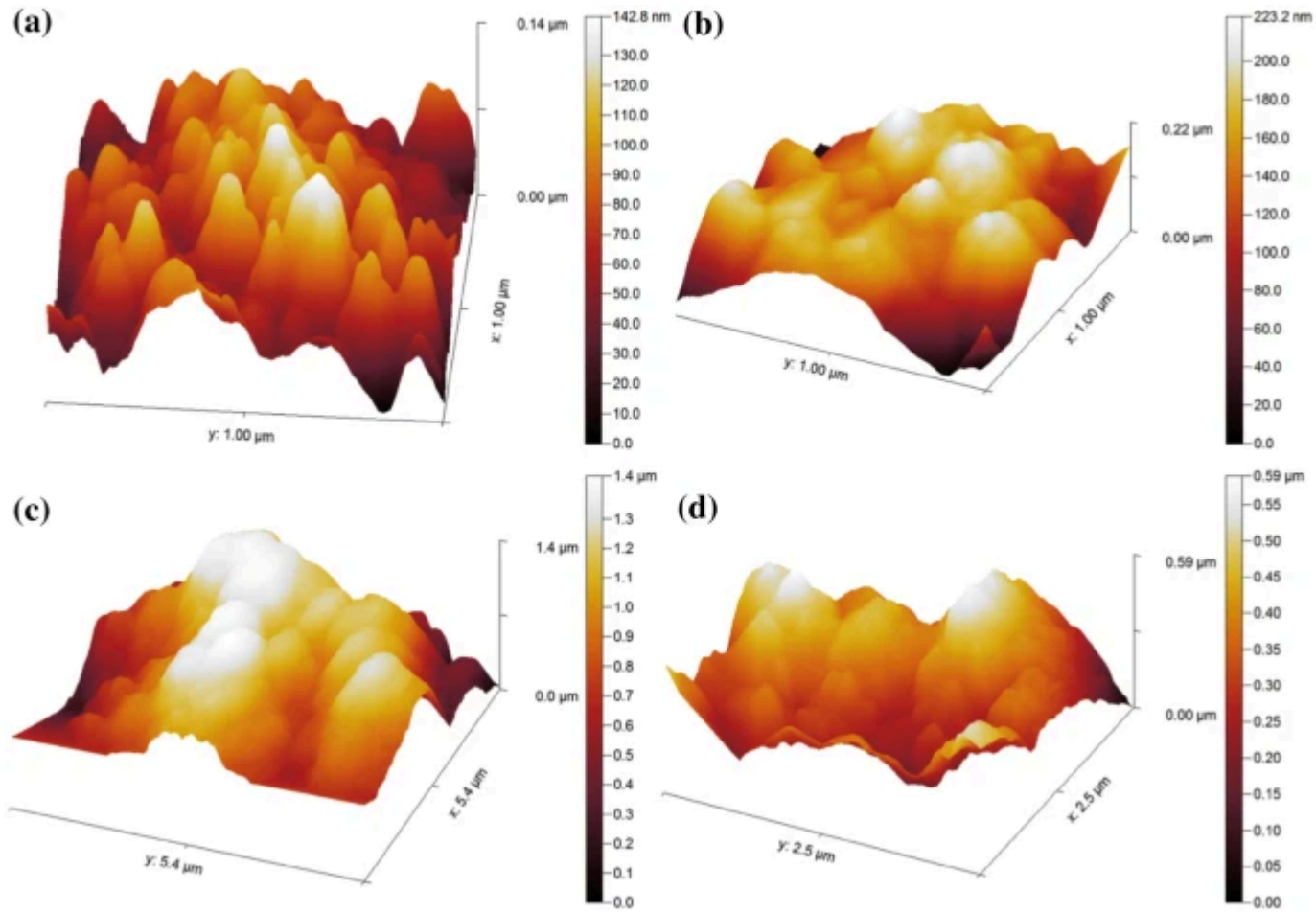

AFM images of **a** Pristine ZnO **b** annealed ZnO **c** PANI/pristine ZnO **d** PANI/annealed ZnO

3.3 Spectroscopic analysis

3.3.1 FTIR spectroscopy

The FTIR spectrum for the pristine ZnO thin films is shown in Fig. 4. The peak frequencies in the spectra and the corresponding possible assignments are shown in the Table 2. The peaks at 2920 cm^{-1} and 2858 cm^{-1} confirms the presence of TEA over the ZnO nanorods, peaks correspond to aliphatic C–H stretching of TEA [20, 21]. The absorption peaks at the wave numbers around 1028 cm^{-1} represents the in-plane and out of plane bending of C–H of TEA in the pristine ZnO thin film. Whereas these peaks disappear after annealing the thin film at 300 °C.

Fig. 4

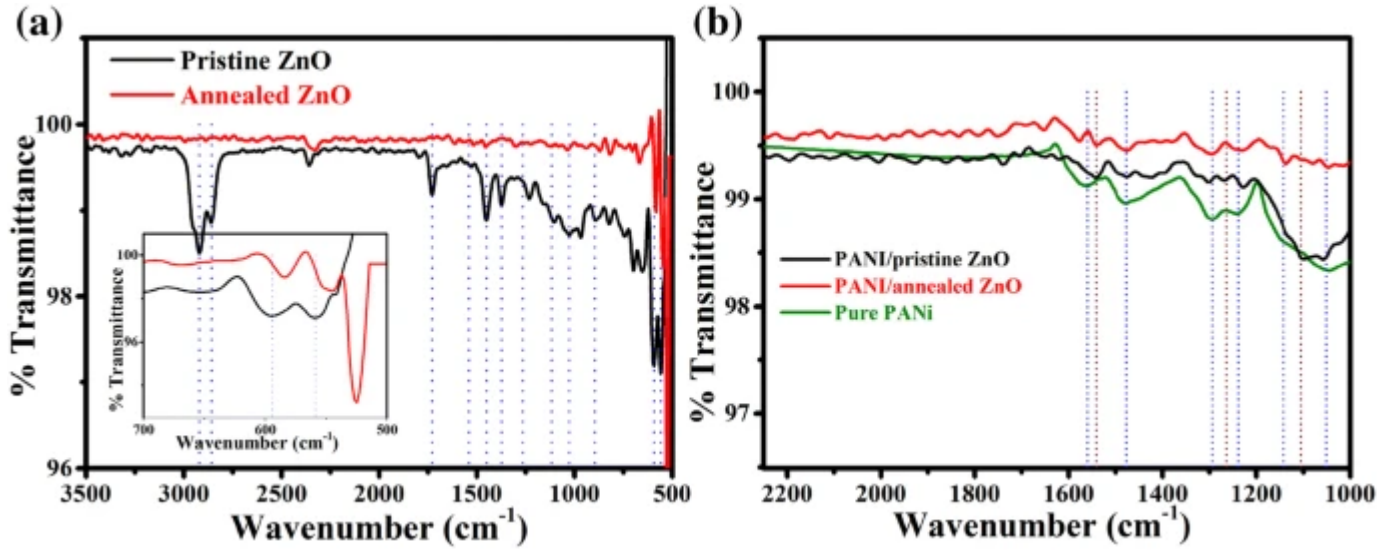

FTIR spectra of **a** pristine and annealed ZnO thin films **b** PANI and PANI coated pristine and annealed ZnO thin films

Table 2 Assignments for peaks in ZnO FTIR spectra

Also from the inset, we can clearly see enhancement in peak intensity at 559 cm^{-1} as well as a shift towards lower wavenumber after annealing. This confirms the complete removal of TEA and after annealing. All the assignments for peaks in ZnO FTIR spectra [20, 21] are tabulated in Table 2.

The FTIR spectra PANI and PANI coated ZnO thin films are shown in Fig. 4b. The characteristic bands for C=C stretching deformation modes of quinoid (Q) and benzenoid (B) rings can be seen at 1580 and 1497 cm^{-1}, the C–N stretching band at 1294 cm^{-1} is assigned to secondary aromatic amine. The C–N–C stretching vibration band is found at 1238 cm^{-1} is the result of in the polaron structure [22]. Bands due C–H out-of-plane bending of 1, 2, 4-substituted rings and C–H out of plane bending of the 1, 2-substituted rings are observed at 1035 cm^{-1} and 690 cm^{-1} respectively. It is expected that the oxide or metal surface strongly interacts with the conjugated structure of PANI, especially through the Q ring (semiquinone radical cation), PANI composite [23]. Once the PANI is coated over the surface of ZnO nanorods, the peaks at 1580, 1294 and 1142 cm^{-1} are found to be

shifted to 1554, 1264 and 1118 cm^{-1}, respectively, implying that the chemical interactions through the semiquinone radical cation between ZnO and PANI [23].

3.3.2 Raman spectroscopy

Raman scattering results of ZnO nanorods thin films both pristine and annealed at 300 °C are shown in Fig. 5a. The observed peak at 333 cm^{-1} for both the samples indicates the E_2 (high)−E_2 (low) mode due to the multi-phonon process, it signifies that the nanorods were single crystals. The peak at 383 cm^{-1} corresponds to the lattice vibration mode of quasi A1 (TO) of ZnO crystal which was more pronounced in the annealed sample then the pristine. The sharp and most pronounced peak at 438 cm^{-1} is attributed to E_2 (high) mode and indicates the high crystalline quality of the nanorods which further confirm the formation of wurtzite ZnO [24]. The Raman spectra intensities and sharpness of E_2 (high) mode increased after annealing suggesting the increase in crystallinity after annealing which is in good agreement with the XRD results. The presence of a small peak at 585 cm^{-1} can be assigned to E_1 (LO) which is attributed to the lattice distortion [24].

Fig. 5

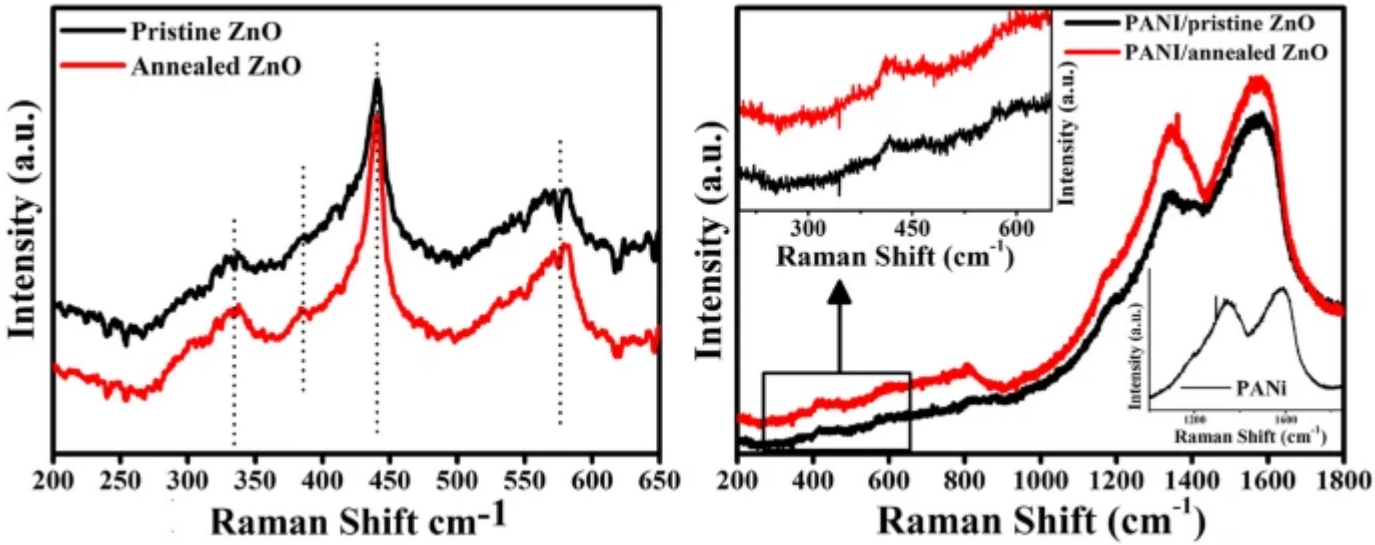

Raman spectra of **a** pristine and annealed ZnO thin film **b** PANI/pristine ZnO and PANI/annealed ZnO thin film

The Fig. 5b shows the Raman spectra of PANI coated pristine and annealed ZnO thin films, while the inset of Fig. 5b shows the Raman spectra of PANI powder. The Raman

spectrum was found to be consistent with previous reports for PANI [25]. The bands at 1170 cm^{-1} and 1590 cm^{-1} can be attributed to benzenoid rings and quinoid segments of PANI, the high-intensity peak at 1331 cm^{-1} confirms the emeraldine salt form of PANI and can be attributed to C–N^+ stretching in PANI [25, 26]. The peaks corresponding to ZnO and PANI can be seen in the Raman spectra for the PANI coated ZnO samples confirming the formation of PANI/ZnO heterojunction.

3.3.3 UV–Vis spectroscopy

The Fig. 6a shows the absorbance spectra of pristine and annealed ZnO thin films, from the spectra we observe a slight increase in absorption near the absorption edge indicating higher crystallinity of the annealed ZnO nanorods thin film. Also, a decreased absorption can be observed in the near IR range of the spectra for the annealed sample, this decrease in absorption can be attributed to a reduction in defects. The bandgap of the pure and annealed thin films was calculated by extrapolating the plot of $(\alpha h\nu)^2$ versus $h\nu$ using the Tauc's relation $(\alpha h\nu)^n = A(h\nu - Eg)$, where α is absorption coefficient and $h\nu$ is photon energy. The inset in Fig. 6a shows the $(\alpha h\nu)^2$ versus $h\nu$ plot of the pristine and annealed samples. A slight increase in bandgap is observed for the annealed thin film, this is due to the quantum size effect as the crystallite size decreases after annealing which is evident from the XRD data. The inset in Fig. 6b shows the absorbance of PANI thin film. The spectrum shows the characteristic absorption peaks for PANI due to π to π^* transition between the benzoid units and formation of polaron in quinoid units at 321 nm and 602 nm respectively [27].

Fig. 6

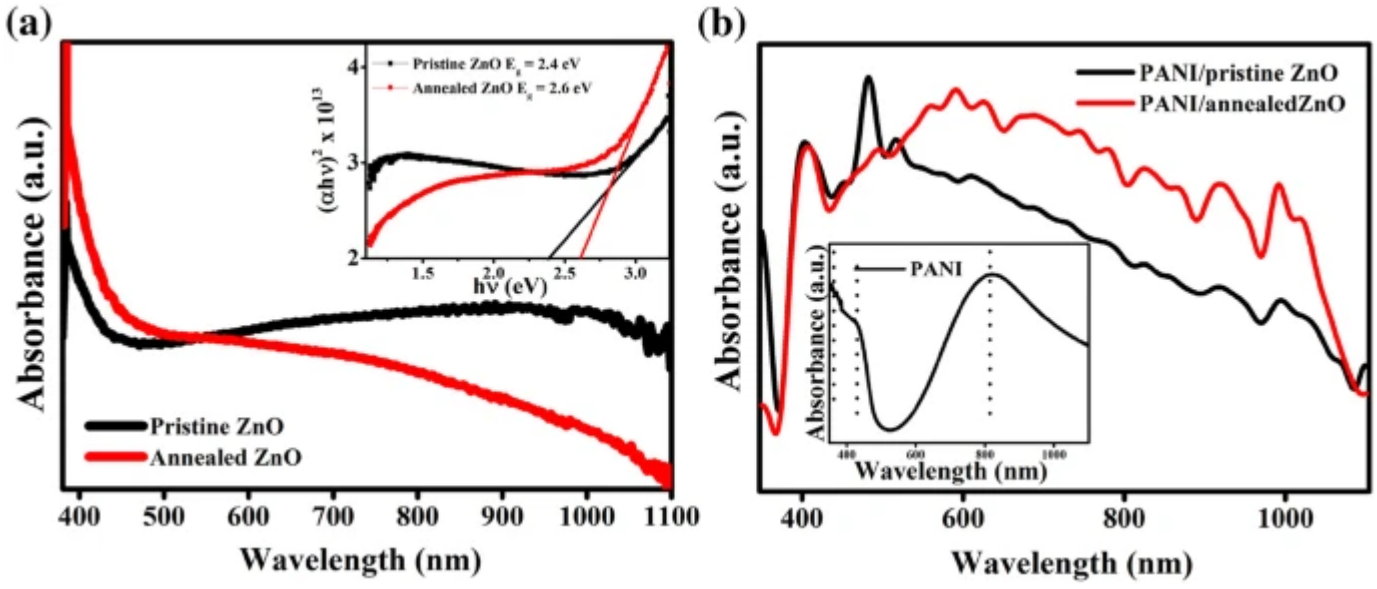

Absorbance spectra and $(ahv)^2$ versus hv plot of **a** pristine and annealed ZnO thin film, **b** PANI coated pristine and annealed ZnO thin film

Figure 6b inset shows the UV–Vis absorbance spectrum of PANI powder, it shows three peaks around 360, 424, and 800 nm which are characteristics of highly doped PANI in its emeraldine salt [27]. The band around 360 nm is due to the π-π* transition of benzoic rings, the peak at 424 nm is attributed to polarons and the peak around 800 nm is due to doping level. The 424 nm peak is an indication that PANI is in salt form (doped) [27].

Figure 6b shows the absorbance spectra of PANI coated pristine and annealed ZnO thin film. From the figure, we observe absorbance onset at 800 nm which dropped to the initial value at around 450 nm and further at lower wavelengths an increase in absorbance is observed. The absorbance spectra confirm the bilayer formation with the spectra covering the entire visible region.

3.4 Electrical analysis

3.4.1 Current–voltage characteristics

Figure 7 shows the current density–voltage characteristics of PANI/pristine ZnO and PANI/annealed ZnO samples. The open circuit voltage V_{oc} was found to be 420 mV and 400 mV for PANI/pristine ZnO and PANI/annealed ZnO samples respectively. While the short circuit photocurrent density J_{sc} was found to be 1.426 mA/cm^2 and 0.818 mA/cm^2 for PANI/pristine ZnO and PANI/annealed ZnO samples respectively.

Fig. 7

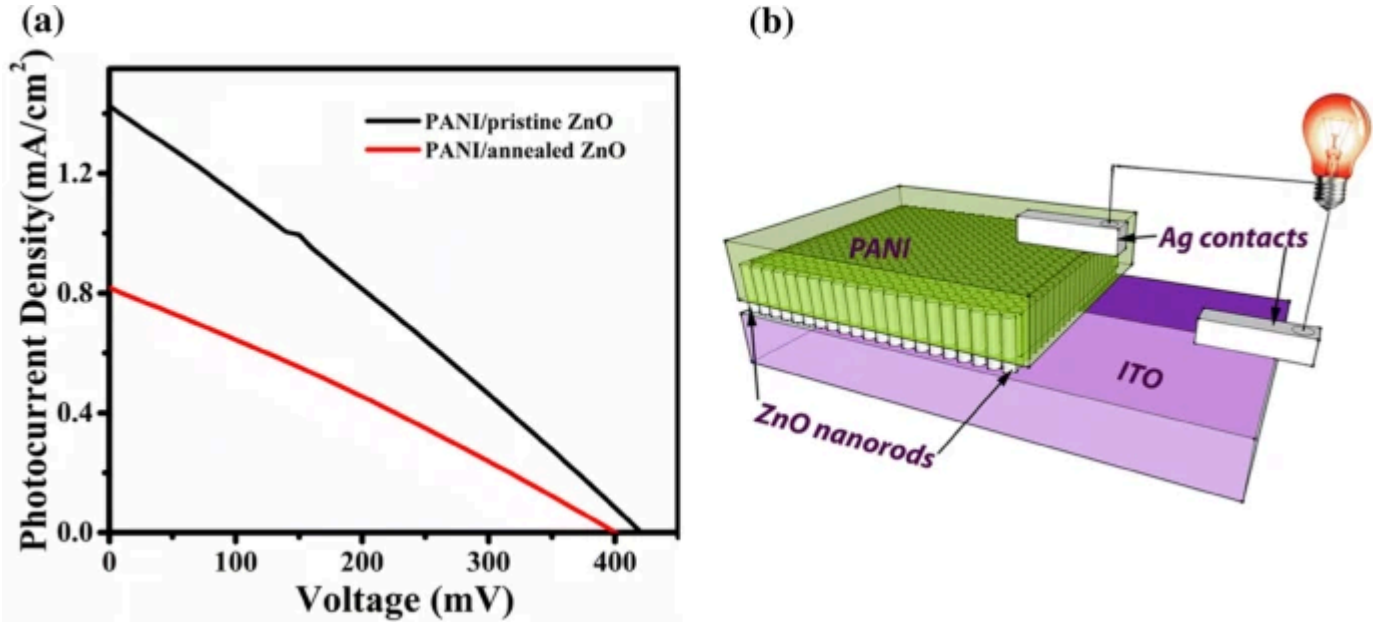

a Current density vs. Voltage characteristics of PANI/pristine ZnO and PANI/annealed ZnO, **b** Schematic of fabricated PANI/ZnO hybrid solar cell

The calculated efficiency was found to be 0.1641% for PANI/pristine ZnO sample which was ~ 80% greater than that for PANI/annealed ZnO i.e. 0.0912%. The decrease in the electrical properties and the solar cell efficiency after annealing of ZnO thin film can be attributed to the change in morphology, surface defects and electronic structure of ZnO thin film.

4 Discussion

The photogeneration and separation of electron–hole pairs is dependent on various factors such as its composition, structure, surface adsorbed functional groups, defects, crystallite size, morphology, aspect ratio etc. [16, 17]. Among these the surface defects are supposed to be trapping centers for the photogenerated holes thereby facilitating electron–hole pair separation. The as-synthesized ZnO thin films show a large number of surface defects evident from the UV–Vis spectroscopy study [18], the surface defects and the aspect ratio have shown a significant decrease after annealing the ZnO nanorods thin films [16]. Furthermore, the space charge region for ZnO nanorods is along its longitudinal direction facilitating the flow of electrons along the length of nanorods thereby decreasing the probability of charge recombination [28]. Thus the decrease in length of nanorods with an increased number of interparticle junctions due to annealing, evident from the FE-SEM analysis has resulted in increased electron–hole recombination [28]. On the other hand PANI being used due to its excellent catalytic activity,

conductivity, color transparency, low cost and a very good charge transporter, the low values of lifetime of charge carriers, excitons, and existence of impurities such as oxygen molecules in PANI results in low values of photo conversion efficiency (PCE) of PANI [23, 29, 30]. Though, the photo response is poor but still the efforts can be made to enhance the overall PCE by optimizing the structural properties of PANI/ZnO interface along with the properties of ZnO and PANI individually. In conclusion, the annealing of the ZnO nanorods thin films resulted in a decrease in surface defects and aspect ratio of the nanorods, while an increase in interparticle junctions together resulted in decreased solar cell efficiency of PANI/annealed ZnO sample.

5 Conclusion

The ultrafast photo induced charge carrier transfer by 1D nanorods morphology of ZnO was obtained by soft chemical route providing high throughput and low cost device production. The 1D ZnO nanorods thin films with c-axis oriented growth of ZnO showed decrease in length on annealing at 300 °C, which further changed the morphology and surface defects. The fabricated hybrid solar cell viz. PANI/pristine ZnO showed ~ 80% a higher efficiency then PANI/annealed ZnO due to the change in morphology as well as increased interparticle junctions after annealing. Thus the study provides a possibility of further improvement in PANI/ZnO hybrid solar cell using 1D morphology.

References

1. K.R.T. Kumar, M. Ramakrishna, G.D. Sukumar, Int. J. Energy Res. **42**, 2305–2319 (2018)

Article Google Scholar

2. R.B. Salikhov, Y.N. Biglova, T.R. Salikhov, Y.M. Yumaguzin, J. Nanoelectron. Optoelectron. **9**, 792–794 (2014)

Article Google Scholar

3. W.J. Ke, G.H. Lin, C.P. Hsu et al., J. Mater. Chem. **21**, 13483–13489 (2011)

Article Google Scholar

4. W.E. Mahmoud, J. Phys. D **42**, 155502 (2009)

Article Google Scholar

5. Ü. Özgür, Y.I. Alivov, C. Liu et al., J. Appl. Phys. **98**, 041301 (2005)

Article Google Scholar

6. B. Cao, W. Cai, J. Phys. Chem. C **112**, 680–685 (2008)

Article Google Scholar

7. L. Li, T. Zhai, Y. Bando, D. Golberg, Nano Energy **1**, 91–106 (2012)

Article Google Scholar

8. N. Mufti, S. Maryam, A.A. Fibriyanti et al., Scanning **2018**, 6545803 (2018)

Article Google Scholar

9. S.M. Hatch, J. Briscoe, A. Sapelkin et al., J. Appl. Phys. **113**, 204501 (2013)

Article Google Scholar

10. J.Y. Ouyang, Acta Phys. Chim. Sin. **34**, 1211–1220 (2018)

Google Scholar

11. J. Jang, J. Ha, K. Kim, Thin Solid Films **516**, 3152–3156 (2008)

Article Google Scholar

12. S.H. Eom, S. Senthilarasu, P. Uthirakumar et al., Sol. Energy Mater. Sol. Cells **92**, 564–570 (2008)

Article Google Scholar

13. O. Lupan, V.M. Guerin, I.M. Tiginyanu et al., J. Photochem. Photobiol., A **211**, 65–73 (2010)

Article Google Scholar

14. S. Tang, N. Tang, X. Meng, S. Huang, Y. Hao, Phys. E **83**, 398–404 (2016)

Article Google Scholar

15. F.H. Alsultany, Z. Hassan, N.M. Ahmed, Superlattices Microstruct. **92**, 68–79 (2016)

Article Google Scholar

16. X. Zhang, J. Qin, Y. Xue et al., Sci. Rep. **4**, 4596 (2014)

Article Google Scholar

17. J. Chang, E.R. Waclawik, CrystEngComm **14**, 4041–4048 (2012)

Article Google Scholar

18. K.P. Gattu, A.A. Kashale, K. Ghule et al., J. Mater. Sci. **28**, 13209–13216 (2017)

Google Scholar

19. J.P. Pouget, M.E. Jozefowicz, A.J. Epstein, X. Tang, A.G. MacDiarmid, Macromolecules **24**, 779–789 (1991)

Article Google Scholar

20. M.A. Haque, S. Mahalakshmi, Mater. Focus **2**, 469–474 (2013)

Article Google Scholar

21. H.R. Liu, G.X. Shao, W. Jia et al., CrystEngComm **15**, 3615–3622 (2013)

Article Google Scholar

22. Z. Zhou, X. Zhang, C. Lu, L. Lan, G. Yuan, RSC Adv. **4**, 8966–8972 (2014)

Article Google Scholar

23. S. Zhu, W. Wei, X. Chen, M. Jiang, Z. Zhou, J. Solid State Chem. **190**, 174–179 (2012)

Article Google Scholar

24. R. Das, A. Kumar, Y. Kumar, S. Sen, P.M. Shirage, RSC Adv. **5**, 60365–60372 (2015)

Article Google Scholar

25. M. Hasan, M.O. Ansari, M.H. Cho, M. Lee, J. Ind. Eng. Chem. **22**, 147–152 (2015)

Article Google Scholar

26. M. Malta, G. Louarn, N. Errien, R.M. Torresi, J. Power Sour. **156**, 533–540 (2006)

Article Google Scholar

27. S. Sharma, S. Singh, N. Khare, Int. J. Hydrog. Energy **41**, 21088–21098 (2016)

Article Google Scholar

28. H.J. Yun, H. Lee, J.B. Joo, W. Kim, J. Yi, J. Phys. Chem. C **113**, 3050–3055 (2009)

Article Google Scholar

29. S. Saha, N. Chaudhary, H. Mittal, G. Gupta, M. Khanuja, Int. Nano Lett. **9**, 127–139 (2019)

Article Google Scholar

30. H.S. Patel, J.R. Rathod, K.D. Patel, V.M. Pathak, R. Srivastava, Adv. Mater. Res. **665**, 239–253 (2013)

Article Google Scholar

Acknowledgements

The authors are thankful to the UGC-DAE Consortium for Scientific Research, Indore and IUAC, New Delhi for the characterization facilities. We are also thankful to the Department of Nanotechnology, Dr B. A. M. University for providing the laboratory facility.

Author information

Authors and Affiliations

Department of Nanotechnology, Dr. Babasaheb Ambedkar Marathwada University, Aurangabad, Maharashtra, 431004, India

Dipak A. Tonpe, Ketan P. Gattu, Vishnu V. Kutwade, Makrand E. Sonawane, Avinash S. Dive & Ramphal Sharma

Corresponding author

Correspondence to Ramphal Sharma.

Additional information

Publisher's Note

Rights and permissions

About this article

Cite this article

Tonpe, D.A., Gattu, K.P., Kutwade, V.V. *et al.* Development of organic/inorganic PANI/ZnO 1D nanostructured hybrid thin film solar cell by soft chemical route. *J Mater Sci: Mater Electron* **30**, 16056–16064 (2019). https://doi.org/10.1007/s10854-019-01976-9

Received	Accepted	Published
16 April 2019	02 August 2019	06 August 2019

Issue Date
September 2019

DOI
https://doi.org/10.1007/s10854-019-01976-9

Share this article